Int. J. Bio-Inorg. Hybr. Nanomater., Vol. 4, No. 2 (2015), 101-111

ISSN Print: 2251-8533
ISSN Online: 2322-4142

International Journal of Bio-Inorganic Hybrid Nanomaterials

Synthesis and Characterization of γ-MnO_2-AgA Zeolite Nanocomposite and its Application for the Removal of Radioactive Strontium-90 (^{90}Sr)

Meysam Sadeghi[1*], Sina Yekta[2], Hamed Ghaedi[3], Esmaeil Babanezhad[4]

[1] Young Researchers and Elite Club, Ahvaz Branch, Islamic Azad University, Ahvaz, Iran
[2] Department of Chemistry, Faculty of Basic Sciences, Islamic Azad University, Qaemshahr Branch, Qaemshahr, Iran
[3] Department of Chemistry, Faculty of Basic Sciences, Bu-Ali Sina University, Hamedan, Iran
[4] Department of Chemistry, Faculty of Basic Sciences, Sharif University of Technology, Tehran, Iran

Received: 17 March 2015; Accepted: 20 May 2015

ABSTRACT

In this scientific research, for the first time, the removal of radioactive strontium-90 (^{90}Sr) by γ-MnO_2-AgA zeolite as a novel nanocomposite adsorbent was accomplished under different conditions such as pH, temperature, adsorbent amount and the contact time that are examined from drinking water of Ramsar city and monitored via Ultra Low-Level Liquid Scintillation Counting (LSC) technique. Prior to the reaction study, this composite was successfully prepared through three steps; first, NaA nanozeolite was prepared by the hydrothermal method. Then, silver ions (Ag^+) were loaded in the NaA nanozeolite framework using ion exchange procedure and silver (I) nitrate solution as silver precursor for the preparation of the AgA nanozeolite. Finally, MnO_2 nanoparticles (NPs) with 19.3 wt% were dispersed and deposited on the external surface of AgA nanozeolite through impregnation method for the preparation of γ-MnO_2-AgA zeolite. The synthesized samples have been characterized and identified using Scanning electron microscopy-energy dispersive micro-analysis (SEM-EDX), X-ray diffraction (XRD) and Fourier transform infrared (FTIR) techniques. The obtained results denoted that radioactive 90Sr was removed and adsorbed by γ-MnO_2-AgA zeolite nanocomposite under optimized conditions including pH= 8.5, temperature (25°C) and adsorbent amount (1.5 g) after 6 h with a yield 93%. The minimum detectable activity (MDA) for ^{90}Sr via LSC instrument was 6.92 mBq/Lit. The counting efficiency of LSC system was 78%. It has been emphasized that γ-MnO_2-AgA zeolite nanocomposite has a high capacity and potential for the removal of radioactive ^{90}Sr.

Keywords: Removal; Radioactive ^{90}Sr; γ-MnO_2-AgA; Zeolite; Nanocomposite; Drinking water.

1. INTRODUCTION

Strontium-90 (^{90}Sr) is an important component of many nuclear wastes and is a high yield fusion product of uranium-235 (^{235}U). It is relatively short-lived with a half-life of 28.8 years. Yttrium-90 isotope (^{90}Y) is its decay product which is β− emitter with half-life of 64 hours and decay energy of 2.28 MeV distributed to an electron, an antineutrino and zirconium-90 (^{90}Zr) which is stable. Strontium isotope ^{90}Sr is treated as

(*) Corresponding Author - e-mail: meysamsadeghi45@yahoo.com

one of the most dangerous products of nuclear fission for human beings [1-5]. For this reason its properties and migration in the environment are widely studied. Drinking and fresh waters usually contain many natural radionuclides: Strontium, tritium, radon, radium and uranium isotopes, etc. It is essential to improve rapid removal and decontamination methods for their determination when considering possible nuclear accidents [6-12].

In the last years there has been an increase in the usage of zeolites in different compositions to delete and bury different radio-contaminations [13]. Zeolites are porous crystalline, hydrated alumina silicates of group IA and IIA elements such as sodium, potassium, barium, magnesium and calcium. One of the most important properties of zeolites is their ability to exchange cations. The type and distribution of cations influence the adsorption behavior of zeolites; thus by ion exchange, sorbent with different molecular sieve and adsorption properties can be prepared [14]. Among these three zeolites, A-type molecular sieve zeolite has attracted more attention because of the higher aluminum content within its crystalline structure [15, 16]. The combination of zeolites and metal oxide nanoparticles renders solid catalysts in which the high surface area of nanoparticles and the absorbent capacity provided by zeolites cooperate to increase the efficiency of the catalytic process [17]. The methods for modifying zeolites are usually by impregnation [18] and ion-exchange [19]. In this research, we have utilized the combination of AgA zeolite as host and MnO_2 nanoparticles as guest materials to synthesize an adsorbent catalyst in which the high surface area of nanoparticles and the absorbent capacity provided by the zeolite cooperation to increase the efficiency of the removal process of ^{90}Sr from drinking water.

Zeolite A exhibits the LTA (Linde Type A) structure. It has a 3-dimensional pore structure with pores running perpendicular to each other in the x, y, and z planes, and is made of secondary building units 4, 6, 8, and 4-4. The pore diameter is defined by an eight member oxygen ring and is small at 4.2Å [20]. The purpose of this research is to investigate the removal of ^{90}Sr by γ-MnO_2-AgA zeolite nanocomposite at room temperature. The present work consists of three parts; the first part includes the preparation of the NaA nanozeolite using hydrothermal method, the second part includes its structure modification by silver-ion exchange using for preparing of AgA nanozeolite. Also, the third part includes is the synthesized γ-MnO_2-AgA zeolite nanocomposite to examine the decontamination of ^{90}Sr in tap water of Ramsar city. To the best of our knowledge, there are no papers reporting the application of γ-MnO_2-AgA zeolite nanocomposite adsorbent used for the removal of ^{90}Sr. Silver cation is the only noble mono-positive cation that forms mononuclear species with appreciable stability in aqueous solution. Besides, silver is known to have strong influence on the absorption properties of zeolites. As an important functional metal oxide, manganese dioxide (MnO_2) is of the most attractive representations of inorganic materials exhibiting such a rich physical and chemical properties and wide applications in various fields such as catalysis, ion exchange, molecular adsorption, biosensor, and energy storage. MnO_2 is a very interesting material because of the diversity in its crystalline structure and high manganese valence [21-23].

2. EXPERIMENTAL

2.1. Materials

Tetra ethyl ortho silicate (TEOS), tetra methyl ammonium hydroxide (TMAOH), aluminum isopropoxide, sodium hydroxide (NaOH), ethanol, silver nitrate ($AgNO_3$), manganese nitrate hexahydrate ($Mn(NO_3)_2.6H_2O$), potassium permanganate ($KMnO_4$), acetone, NaOH and HNO_3 were purchased from Merck (Merck, Darmstadt, Germany). The high-capacity cocktail OptiPhase HiSafe-3 (Wallac Oy, Turku, Finland) and double-distilled water were used throughout the work. A strontium standard source with activity of 736.5 Bq/mL was utilized as stock solution that desirable diluted solutions with certain activity were prepared subsequently. Deionized water was used for the preparation of all the solutions.

2.2. Preparation of sodium A-type (NaA) nanozeolite by the hydrothermal method

For this work, aluminate and silicate solution were prepared according to the following procedure. 10.5 g of NaOH pellets and 12 g of tetra methyl ammonium

hydroxide (TMAOH) were together dissolved in 100 mL de-ionized water, in which aluminum isopropoxide (8 g) was added later. The resulting mixture was stirred until a clear solution was formed (solution A). Separately, 16 g of tetra ethyl ortho silicate (TEOS) was added to the rest of the required amount of TMAOH and ethanol solution. The resulting mixture initially formed an emulsion-like state under stirring. However, after 2h of continuous stirring, a homogeneous and clear solution was formed (solution B). Mixing of solutions A and B under stirring was resulted the initial clear solution for synthesis. In order to assure the formation of initially clear solutions free from cloudy particles of gel, the solutions were typically stirred for 3 h at room temperature. Then, hydrothermal crystallization of the zeolite was carried out at 98°C for 50 h. Finally, zeolite nanoparticles were recovered from the mother liquor by centrifuge at 10000 rpm for 40min. In order to remove un-reacted materials, the powder was dispersed in DI water by sonication and centrifuged again. This procedure was repeated until the pH of the supernatant decreased to lower than 8. Then the powder was dried at 65°C overnight. The as-synthesized nanozeolitic powders were calcined in oven at 500°C in 4h with the heating and cooling rate of 1°C/min to remove TMAOH molecules [24].

2.3. Preparation of silver A-type (AgA) nanozeolite by the ion exchange method

In a typical procedure, 1.5 g of the synthesized NaA nanozeolite before ionic exchange was calcined at 400°C for 3 h in a furnace for excluding moister and impurities from the surface. The calcined NaA nanozeolite was then added to a 50 mL of a 0.1 M silver nitrate ($AgNO_3$) solution and the mixture was magnetically stirred at 60°C for 5 h to perform ion exchange process in which Ag^+ ions were replaced Na^+ ions. The resulting zeolite was filtered and washed with deionized water to remove the excess salt ions, then dried at 110°C for 16 h. Finally, the clean and dry nanozeolite was calcined in a furnace at 400°C for 4 h [25].

2.4. Preparation of γ-MnO_2-AgA zeolite nanocomposite by the impregnation method

The incorporation of MnO_2NPs loaded onto AgA nanozeolite (γ-MnO_2-AgA) was performed by the impregnation method. First, 1 g of AgA nanozeolite was poured into a 20 mL of 1 M ($Mn(NO_3)_2$) aqueous solution and stirred for 5 h. Under continuous stirring, 50 mL of a 0.2 M ($KMnO_4$) solution was added to the mixture rapidly. $KMnO_4$ has been known among the strong oxidizing agents [26], so that, the color of the solution immediately turned to dark brown, indicating the formation and precipitation of MnO_2NPs through oxidation with $KMnO_4$. The obtained sample was then dried at 100°C for overnight. At last, the product was treated by calcination at 500°C for 4 h [27-30]. The ionic equation of the reaction is as follows (1):

$$3Mn^{2+} + 2MnO_4^- + 2H_2O \rightarrow 5MnO_2 + 4H^+ \quad (1)$$

2.5. Procedure of radioactive ^{90}Sr removal by γ-MnO_2-AgA zeolite nanocomposite

For radioactive ^{90}Sr removal study, the amounts of adsorbent (0.5-3 g) was added to 150 mL of the drinking water spiked with ^{90}Sr at pH= 2.5-8.5 and the mixture were stirred for 1, 2, 3, 6 and 10 h, respectively. After filtration of the mixture, 5 mL of supernatant solutions were analyzed by liquid scintillation spectrometry (LSC) and the activities of the aqueous phase were determined. In LSC, an aliquot of the sample is put into a vial and mixed homogeneously with 15 mL of scintillation cocktail. A shaker was utilized for mixing of cocktail and sample. Samples and cocktail were mixed in 20 mL polyethylene vials, Poly vial. The outside of the vials was cleaned with acetone. All of the polyethylene vials were stored in a cool, dark shield for 2 h to eliminate the scintillation cocktail fluorescence. All samples were counted by LSC for 5 h. The initial source activity was 736.5 Bq/mL as mentioned above that 260 µL of it (equal to 60 Bq) was added to solution samples and the relative error of radioactivity measurements did not exceed 2%.

2.6. Characterization technique

Physicochemical characterizations of the samples with different analytical techniques were performed. SEM images using a scanning electron microscope coupled with energy dispersive X-ray spectrometer (SEM-EDX, HITACHI S-300N). The crystallinity of the samples was determined by X-ray diffraction (XRD) analysis on a Philips X-ray diffractometer using cobalt

(Co) radiation (40 kV, 30 mA and λ= 0.15418 nm). Samples were scanned at 2°/min in the range of 2θ= 080°. The IR spectrum was scanned using a Perkin-Elmer FTIR (Model 2000) in the wavelength range of 400 to 4000 cm^{-1} with KBr pellets method. An ultra-low level liquid scintillation counter (1220 Wallace Quantulus), Perkin Elmer USA) has been used for all measurements. The high-capacity cocktail OptiPhase HiSafe-3 (Wallac Oy, Turku, Finland) and double-distilled water were used throughout the work. A strontium standard source with activity of 736.5 Bq/mL was utilized as stock solution that desirable diluted solutions with certain activity were prepared subsequently.

3. RESULTS AND DISCUSSION

3.1. Scanning electron microscopy (SEM) Analysis

The crystalline size and morphology of the as-syn-

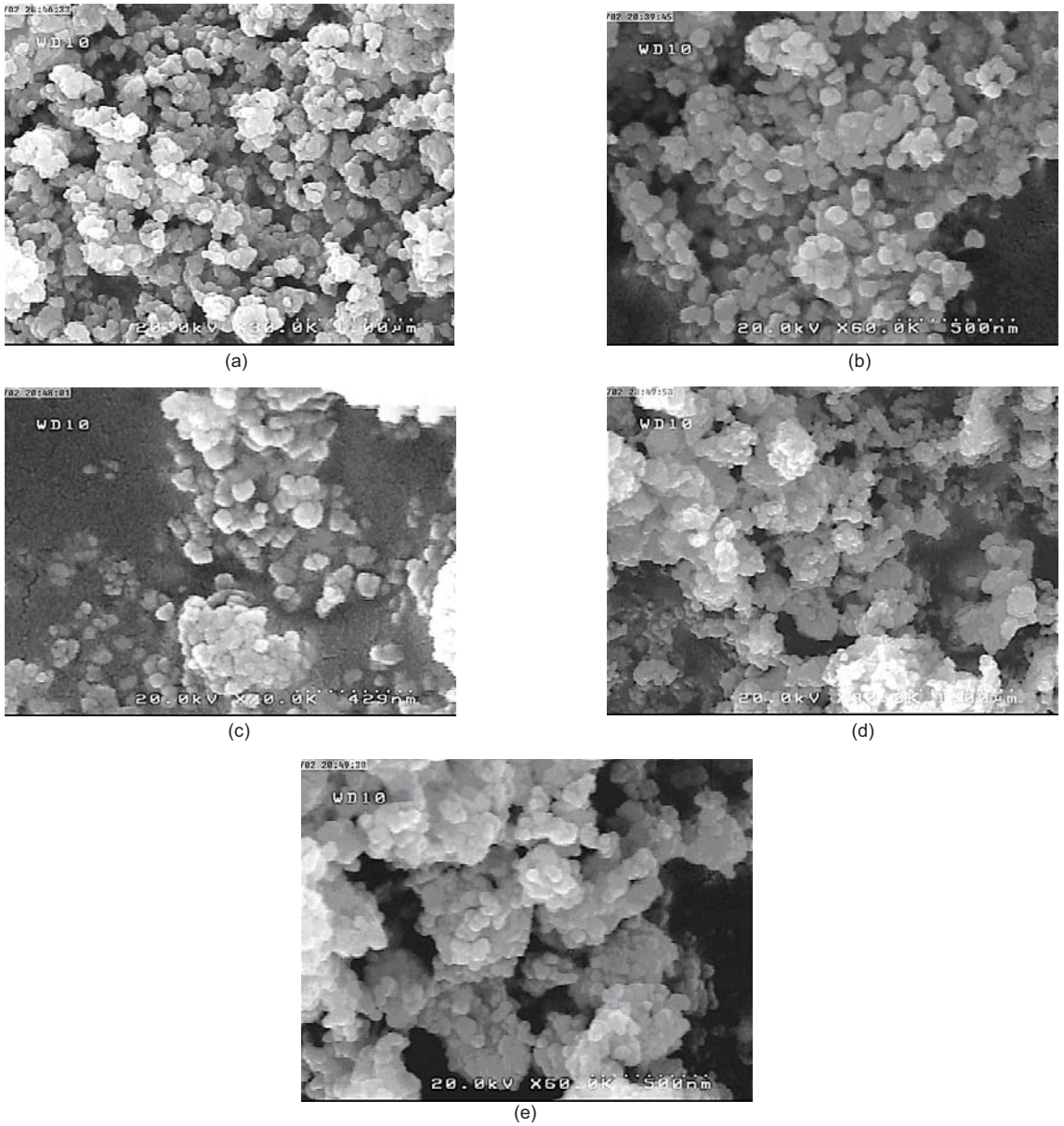

Figure 1: *SEM images of the synthesized samples: (a) NaA, (b) and (c) AgA, (d) and (e) γ-MnO_2-AgA with different magnification.*

thesized samples were surveyed through magnification by SEM images (Figure 1). Comparison between the morphologies of NaA and AgA nanozeolites and γ-MnO_2-AgA zeolite nanocomposite demonstrates the homogeneous morphology of the structures. In addition to this, it shows that the cubic morphology and crystalline size of NaA nanozeolite (Figures 1a) are almost retained with ion exchange process which is indicated by SEM images in Figures 1b and 1c. Although, it can be seen that the crystal structure of γ-MnO_2-AgA zeolite nanocomposite (Figures 1d and 1e) slightly changed as compared to support AgA nanozeolite (Figures 1b and 1c). The average crystalline size of zeolites was illustrated to have nano-metric dimensions (less than 100 nm).

3.2. Energy-dispersive X-ray spectrometer (EDAX) analysis

Figure 2 give the composition elements present in γ-MnO_2-AgA zeolite nanocomposite were investigated by energy dispersive X-ray (EDAX) analysis. In the EDAX spectra, the appeared peaks in the regions of approximately 0.55, 1.15, 1.50, 1.75 and 2.92 and 3.21 keV are corresponded to the binding energies of oxygen (O), sodium (Na), aluminum (Al), silicon (Si) and silver (Ag) respectively that are related to the AgA zeolite. On the other hand, in spectrum (Figure 2b), the appeared two peaks in the regions of 5.86 and 6.24 keV are related to the binding energies of manganese (Mn) which reveals the presence of Mn in the composite. These results confirm coexistence of 6 wt% and 19.3 wt% silver and manganese in the prepared sample, respectively.

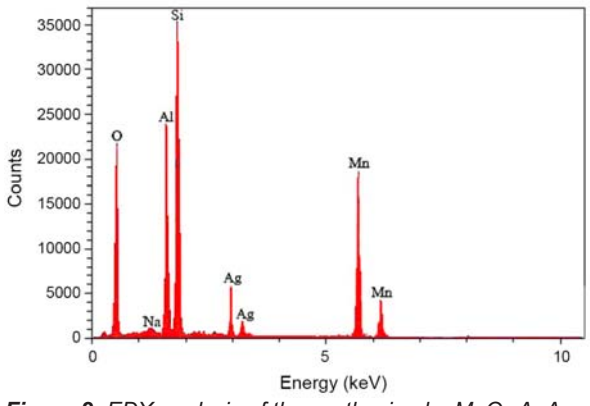

Figure 2: *EDX analysis of the synthesized γ-MnO_2-AgA.*

3.3. X-ray diffraction (XRD) analysis

In Figure 3, XRD patterns of the under study NaA and AgA nanozeolites and γ-MnO_2-AgA zeolite nanocomposite are displayed, respectively. As seen from the patterns, the sharp peaks referring to NaA nanozeolite occurred at scattering angles 8.3903°, 11.8550°, 14.5154°, 16.2328°, 18.7716°, 25.2498°, 27.9694°, 28.2933°, 31.6463°, 34.9609°, and 39.9286° corresponding to the diffraction planes of (2 2 0), (2 2 2), (4 0 0), (4 2 0), (4 2 2), (4 4 4), (6 4 2), (8 0 0), (6 6 2), (9 3 1) and (10 4 2), which have been crystallized in the cubic system and are in good agreement with those of NaA nanozeolite with molecular formula of $Na_6[AlSiO_4]_6.4H_2O$ with reference code (ICDD) of 00-042-0216. NaA zeolite structure was retained even after silver cation exchange in AgA nanozeolite (ICDD= 01-079-0347) with molecular formula of $Ag_8Al_{12}Si_{12}O_{48}.2H_2O$. Meanwhile, synthesized MnO_2NPs (as guest material) loaded as a 19.3 wt % of unit onto AgA zeolite as the host material, possesses a series of new peaks which were obtained at 2θ of 34.644°, 41.995°, 53.753°, and 63.689° corresponding to the diffraction planes of (1 3 1), (3 0 0), (1 6 0) and (4 2 1), respectively. No characteristic peaks related to the presence of impurities were observed in the patterns during MnO_2 loading. These peaks which are illustrated as red points in Figure 2c reveal that MnO_2NPs have been dispersed and deposited onto AgA nanozeolite and also indicate a host-guest interaction between AgA framework and MnO_2NPs. A definite line broadening of the scattering pattern in Figure 2c is a demonstration upon which the synthesized MnO_2 particles are in nanoscale range. However, a small loss of crystallinity is observed in Figures 2b and 2c associated with the lower intensity of the peaks at 2θ of 11.630° and 18.318°. This may occur because of the dealumination process of AgA nanozeolite and γ-MnO_2-AgA zeolite nanocomposite and associated with the location of substituted silver and impregnated manganese cations. The Mn^{4+} ions within the zeolite framework can interact with the aluminate sites more strongly than that of Na^+ or Ag^+ ions. Totally, it can be concluded that with silver ion exchange in NaA nanozeolite and subsequent loading of MnO_2NPs onto AgA nanozeolite, the structure of the zeolites did not change. On the other hand, the ca-

pacity of the A-type zeolite to keep the guest species is limited. Consequently, the adsorption of the host cations (Si, Al and Na) will stop if the capacity is filled. In contrast, the amount of the host species in the AgA nanozeolite increases with increasing the manganese dioxide content. The introduced MnO_2NPs were dispersed and deposited on the external surface of AgA nanozeolite, however, due to the relative aggregation during processing of the composite, some particles are too large to perch inside the structure. Hence, high MnO_2NPs loading will cause structural damage to the zeolite. The size of the prepared MnO_2NPs deposited onto AgA nanozeolite was also investigated via XRD measurement and line broadening of the peak at 2θ= 0°-80° using Debye-Scherrer equation (2) [31]:

$$d = \frac{0.94\lambda}{\beta \cos\theta} \quad (2)$$

Where d is the crystal size, λ is the wavelength of X-ray source, β is the full width at half maximum (FWHM) and θ is Bragg diffraction angle. Using this equation, the average particle size for AgA nanozeolite and MnO_2NPs are estimated to be 25.7 and 6 nm, respectively. The particle size obtained from XRD measurement is consistent with the results from the SEM study.

3.4. FTIR study

The characterization of the prepared samples along with the A-zeolite precursors was further surveyed by FTIR spectra as plotted in Figure 4. The FTIR spectrum in transmittance mode in Figure 4 shows peaks at 462, 558, 669, 755, 986, 1644 and 3440 cm^{-1}, respectivedy. All of the two as-synthesized typical samples, namely NaA and AgA nanozeolites have peaks around 462 cm^{-1} and 558 cm^{-1} which are assigned to the bonding vibration of the insensitive internal TO_4 (T= Si or Al) tetrahedral units and the double ring external linkage within the A zeolite structure, respectively. The peaks at 669 cm^{-1} and 755 cm^{-1} are attributed to external linkage and internal tetrahedral symmetrical stretching vibrations (D6R), respectively. Furthermore, the peaks at 986 cm^{-1} is corresponded to internal tetrahedral asymmetrical stretching vibrations, and the peaks around 1644 cm^{-1} and 3440 cm^{-1} are assigned to H–O–H bending and O–H bonding

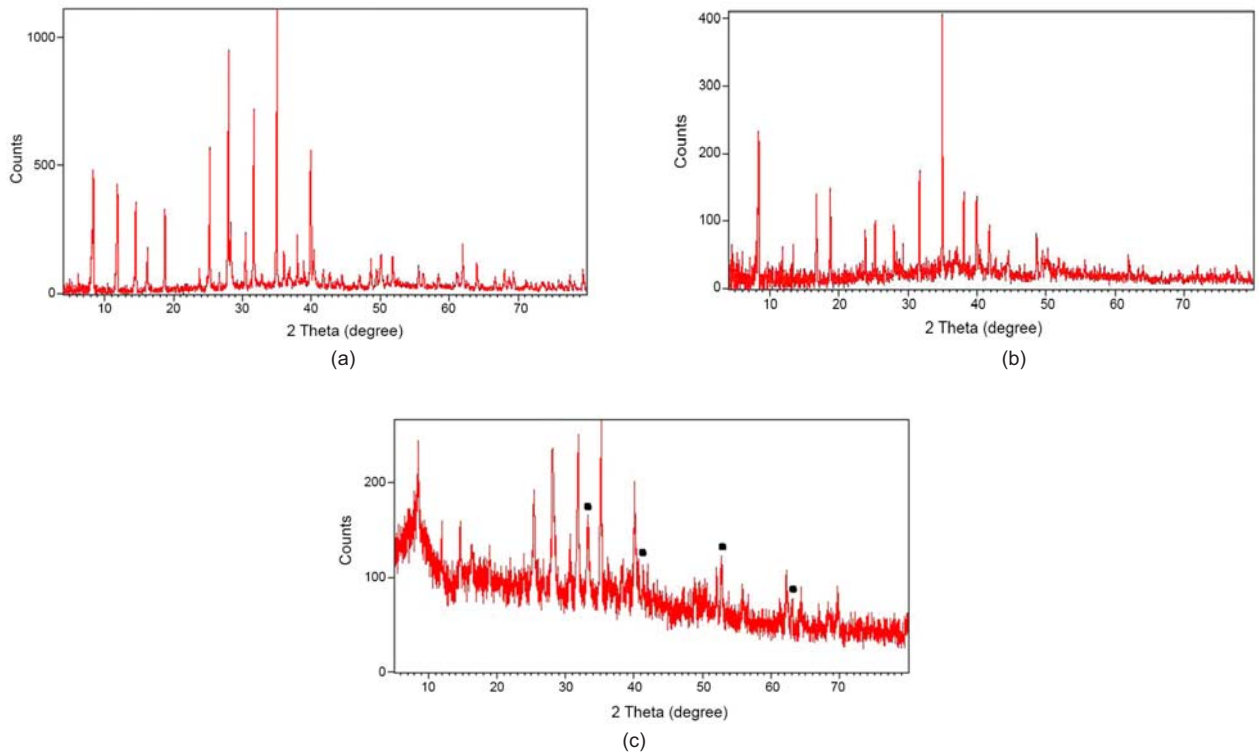

Figure 3: *XRD patterns of the synthesized samples: (a) NaA, (b) AgA and (c) γ-MnO_2-AgA.*

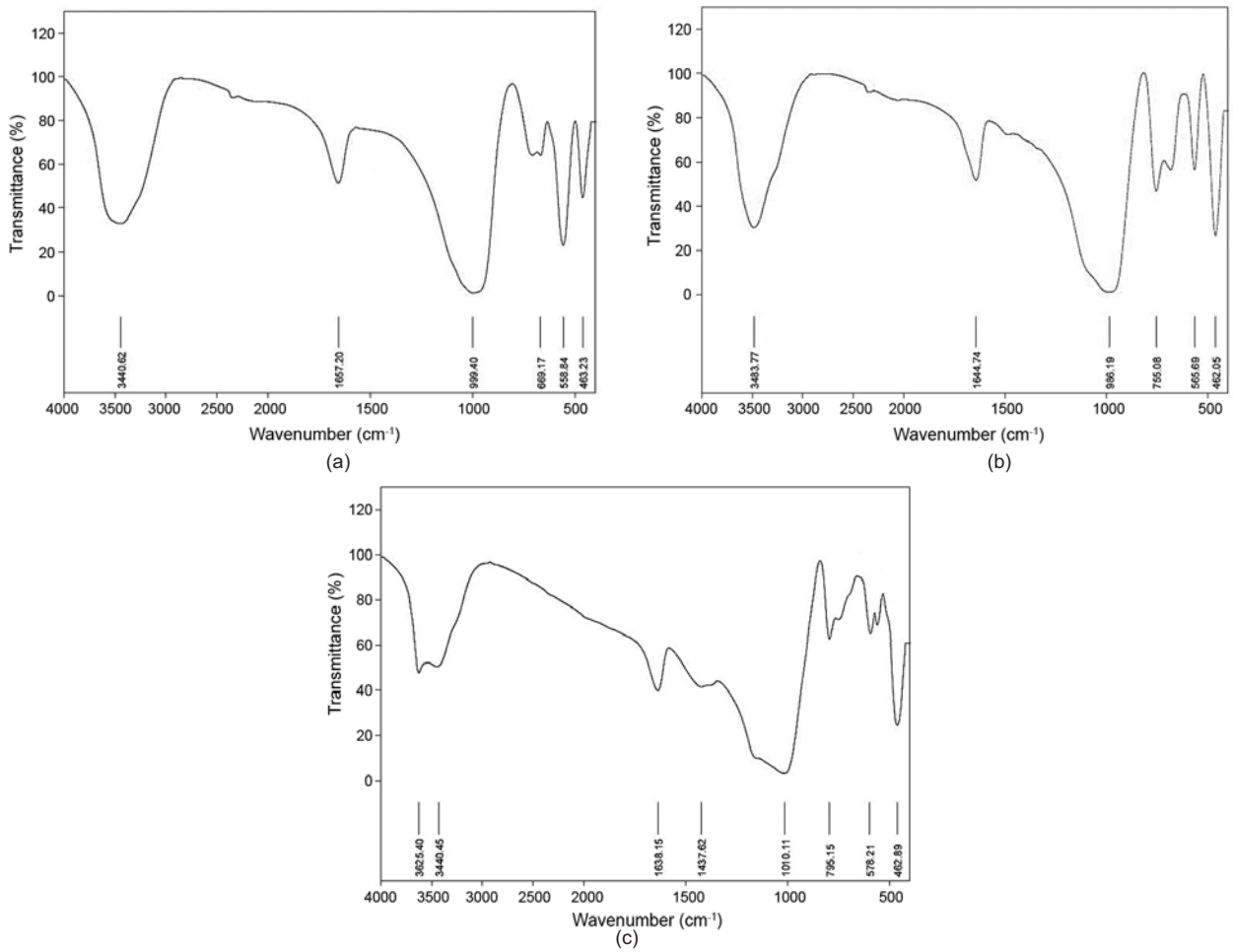

Figure 4: *FTIR spectra of the synthesized samples: (a) NaA, (b) AgA and (c) γ-MnO_2-AgA.*

(hydroxyl groups) vibrations of A zeolite structures, respectively. Comparing Figure 4a and 4b confirms that no changes has occurred in the bands of AgA zeolite compared with the original NaA zeolite, which tends to lend further support to the idea that the ion exchange modification of NaA zeolite by silver ion has a very little influence on the chemical structure of the zeolite framework. On the other hand, Figure 4c illustrates three new peaks related to the synthesized loaded MnO_2NPs. The absorption peak at 578 cm^{-1} is corresponded to Mn–O bond. The peaks around 1437 cm^{-1} and 3625 cm^{-1} are attributed to H–O–H bending and O–H bonding (hydroxyl groups) vibrations of the nanoparticles, respectively.

3.5. Removal study of ^{90}Sr by MnO_2NPs-AgA zeolite composite

In order to investigate the removal and adsorption of radioactive ^{90}Sr, the adsorbent performance of γ-MnO_2-AgA zeolite nanocomposite adsorbent were evaluated and those progresses were monitored by Ultra low-level liquid scintillation spectroscopy. The various conditions including pH, temperature, adsorbent amount and the contact time were surveyed and optimized.

3.5.1. Effect of pH

One of the most significant parameters that affect the sorption process of radioactive ^{90}Sr is the pH of the considered solution. The role of pH on the adsorption yield of γ-MnO_2-AgA zeolite nanocomposite adsorbent was studied via utilizing ^{90}Sr solution of 58.44 Bq at optimized temperature (25°C) for 6 h. As represented in Figure 5, the adsorption properties of ^{90}Sr was studied at pH ranges of 2.5-10.5 on the removal of ^{90}Sr by nanocomposite adsorbent. To achieve the

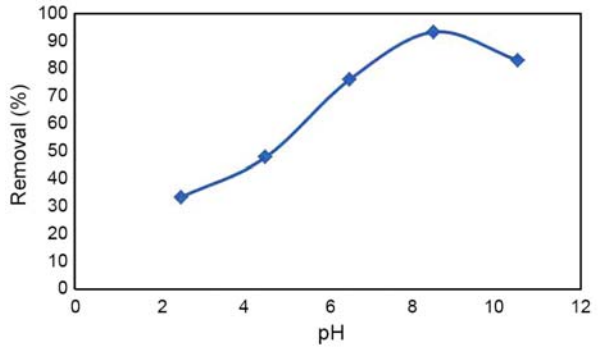

Figure 5: *The curve of ^{90}Sr removal% versus pH.*

most selectivity and removal efficiency, pH of 8.5 was considered for the further modifications and 93% adsorption yield. The solution pH was adjusted via 1M solutions of NaOH and HNO_3. Moreover, the sorption equilibrium was reached, the supernatant solution of ^{90}Sr were brought out and introduced to the Ultra Low-Level Liquid Scintillation Counter (LSC). Subsequently, the adsorption and removal value percentage of ^{90}Sr by composite adsorbent was calculated. The interaction of hydrogen ions with an oxygen radical of the zeolite body generates hydroxyl groups and lowers the charge of the matrix, which is accompanied by a decrease in the sorption ability of nanocomposite in relation to ^{90}Sr. Besides, a higher sorption of the radionuclide due to increasing pH shows that in the solution they are in an ionic state.

3.5.2. Effect of temperature

The temperature in which the experiment fulfills is a significant parameter that cannot be over looked. In this research, the adsorption of radioactive ^{90}Sr on the γ-MnO_2-AgA zeolite nanocomposite adsorbent was investigated in the temperature range of 25-45°C under optimized conditions. Figure 6 illustrates the effect of temperature on the adsorption of ^{90}Sr on the nanocomposite adsorbent surface. As can be seen, the adsorption of ^{90}Sr on the γ-MnO_2-AgA zeolite nanocomposite adsorbent decreases as the temperature increases gradually. This is why in high temperatures the formed bonds between ^{90}Sr and active sites of adsorbent will be weak and break down eventually.

3.5.3. Effect of amount of adsorbent

The selection of appropriate amounts of adsorbent is a key role that affects the whole removal process. The adsorption properties of radioactive ^{90}Sr were evaluated at ranges of 0.5-3 g on the removal of ^{90}Sr by composite adsorbent. As it has been shown in Figure 7, with increasing of adsorbent amount, the removal efficiency increases, until the point after which no more significant variations is seen and the curve slope tend to a linear form which means constant values. Thus, 1.5 g was chosen as the appropriate mass for γ-MnO_2-AgA zeolite nanocomposite adsorbent to fulfill high yield removal.

3.5.4. Effect of contact time

In order to provide a logical comparison between adsorption capability of γ-MnO_2-AgA zeolite nanocomposite adsorbent and reaction time, the effect of various contact time intervals on the adsorption of radioactive ^{90}Sr was accomplished. The diversity of adsorption value (%) with shaking time has been explained in Figure 8. Figure 8 represents the reliability of adsorption yield of ^{90}Sr on the nanocom-

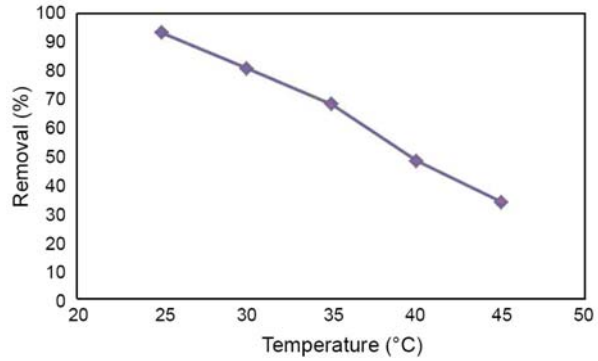

Figure 6: *The curve of ^{90}Sr removal% versus temperature (°C).*

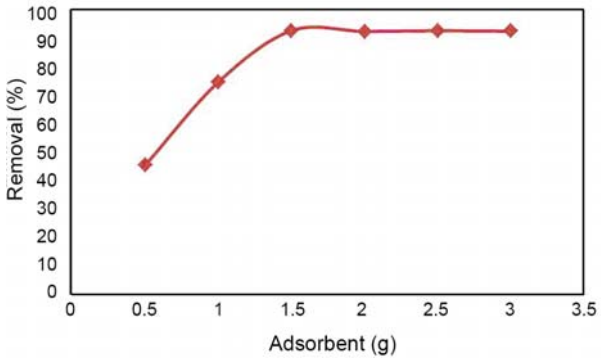

Figure 7: *The curve of ^{90}Sr removal% versus adsorbent amount.*

posite adsorbent to the contact time. As the reaction time increases, the adsorption will increase slightly. The adsorption time was investigated in the range of 1–10 h and LSC analysis showed that the removal first increased up to 6 h and then remained constant. Thus, to achieve a shorter analysis time 6 h was chosen as optimum value. The obtained results from designed experiment denoted that the sorption procedure was rapid and equilibrium gained quickly after mixing the composite adsorbent with target containing solution. ^{90}Sr uptake on the γ-MnO_2-AgA zeolite nanocomposite adsorbent may be the cause of exchange of target metallic ion with the other ions presented on the adsorbent surface. The Liquid scintillation counting (LSC) spectra for removal of ^{90}Sr as count versus channel and count versus energy are represented in Figures 9 and 10, respectively. In these spectra, the energetic window A (150-760) includes all the ^{90}Sr spectrum and low energy region of ^{90}Y spectrum. The window B (760-940) includes the high-energy region of the ^{90}Y spectrum. ^{90}Sr analysis of natural water sample from the Ramsar city of Iran has been performed. A typical spectrum of ^{90}Sr in equilibrium with its daughter (^{90}Y)

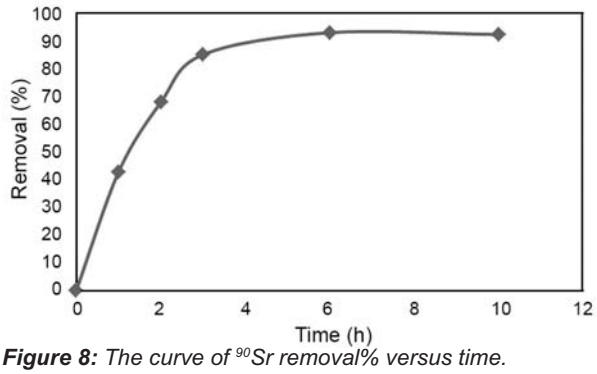

Figure 8: *The curve of ^{90}Sr removal% versus time.*

is shown in Figure 8. The strontium activity was calculated using the following equation (3):

$$A_{Sr} = \frac{(I_{G,A} - I_{BKG,A}) - (I_{G,B} - I_{BKG,B})F_Y}{60 \times E_{Sr} \times R_{Sr} \times V_w} \quad (3)$$

Where is the ^{90}Sr activity in Bq/L; $I_{G,A}$ the gross count rate in region A (channels 150-760) in counts per minute (CPM); $I_{BKG,A}$ the background count rate in region A in CPM; $I_{G,B}$ the gross count rate in region B (channels 760-940) in CPM; $I_{BKG,B}$ the background count rate in region B in CPM; F_Y the correction factor taking into account the ^{90}Y contribution to the ^{90}Sr

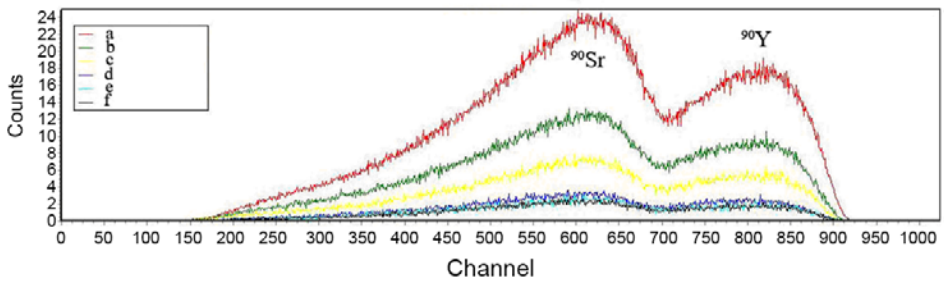

Figure 9: *Liquid scintillation counting (LSC) spectra for removal of ^{90}Sr (count versus channel), (a) before contacting with prepared γ-MnO_2-AgA zeolite nanocomposite adsorbent , b) 1h, (c) 2h, (d) 3h, (e) 6h and (f) 10h.*

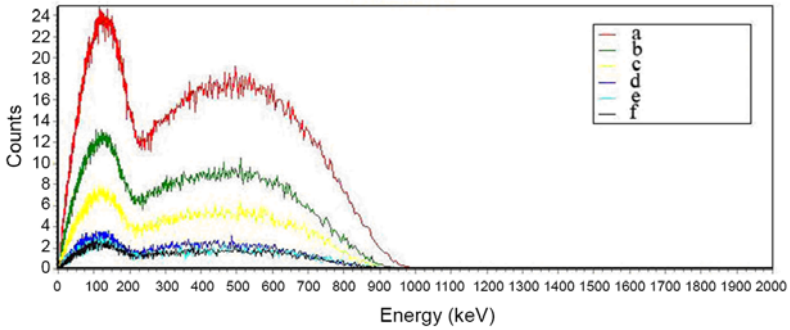

Figure 10: *Liquid scintillation counting (LSC) spectra for removal of ^{90}Sr (count versus energy), (a) before contacting with prepared γ-MnO_2-AgA zeolite nanocomposite adsorbent, (b) 1h, (c) 2h, (d) 3h, (e) 6h and (f) 10h.*

Table 1: *Liquid scintillation counting (LSC) results for removal of ^{90}Sr by γ-MnO_2-AgA zeolite nanocomposite adsorbent.*

Time (h)	CPM(A)	CPM(B)	Activity (Bq/Sample)	Count. Time Min.	MDA (mBq/Sample)
0	6005.56	2890.41	58.44	100	6.92
1	3225.81	1471.62	33.46	100	6.92
2	1850.58	860.50	18.75	100	6.92
3	819.48	364.92	8.69	100	6.92
6	598.66	277.06	4.06	100	6.92
10	632.23	291.23	4.45	100	6.92

window; and F_Y is derived from where $I_{Y,A}$ is the gross count rate of ^{90}Y in region A in CPM and $I_{Y,B}$ is the gross count rate of ^{90}Y in region B in CPM. E_{Sr} the ^{90}Sr LSC efficiency R_{Sr} the chemical recovery factor; V_w the mass of dried sample in kg;

The minimum detectable activity (MDA) was evaluated using Currie formula (4) and (5) [32]:

$$MDA(Bq/kg) = L_d(\varepsilon TQ)^{-1} \quad (4)$$

$$L_d(counts) = 2.71 + 4.65(BT)^{-1/2} \quad (5)$$

Where ε parameter is the detection efficiency; T parameter is the counting time (s); Q parameter is the sample quantity (kg) and B parameter is also the background count rate (s^{-1}).

The removal reaction efficiency percentage was also calculated using the following equation (6):

$$Removal(R\%) = \frac{(A0 - A_e)}{A_e} \times 100 \quad (6)$$

Where A_0 and A_e are the ^{90}Sr activities in the aqueous phase before and after sorption.

4. CONCLUSIONS

In summary, γ-MnO_2-AgA zeolite nanocomposite was successfully synthesized and applied for the removal of radioactive ^{90}Sr ions from drinking water of Ramsar city. The synthesized adsorbent was characterized by SEM/EDX, XRD and FTIR techniques and the removal process followed via Ultra Low-Level Liquid Scintillation Counting (LSC) analysis. The different conditions such as pH, temperature, adsorbent amounts and the contact time were investigated and optimized. The results denoted that γ-MnO_2-AgA zeolite nanocomposite adsorbent has higher surface area that leads to removal of ^{90}Sr. The pH= 8.5, temperature (25°C), adsorbent amount (1.5 g) and contact time (6 h) were optimized conditions for this process. By consideration of high potential of this composite adsorbent, it can be used for removal of other radionuclide elements which may happen to the environmental water samples.

ACKNOWLEDGEMENT

The financial support of the Laboratory at the Imam Hussein Comprehensive University (IHCU), Tehran is gratefully acknowledged.

REFERENCES

1. Zhu S., Ghods A., Veselsky J.C., Mirna A., Schelenz R., *Radiochima. Acta*, **8** (1990), 195.
2. Chegrouche S., Mellah A., Barkat M., *Desalination*, **235** (2009), 306.
3. Sebesta F., Motl John A.J., Proceedings of International. Conference on Nuclear Waste Management and Environmental Remediation, Prague, **3** (1993), 871.
4. Mardan A., Ajaz R., Mehmood A., Raza S.M., Ghaffar A., *Sep. Purif. Technol.*, **16** (1999), 147.
5. Mardan A., Ajaz R., *J. Radioanal. Nucl. Chem.,* **251** (2002), 359.

6. Szeglowski Z., Constantinescu O., Hussonnois M., *Radiochima Acta*, **64** (1994), 127.
7. Abadzic, S.A., Ryan, J.N., *Environ. Sci. Technol.*, **35** (2001), 4502.
8. Furhmann M., Aloysius D., Zhou H., *Waste Manage*, **15** (1995), 485.
9. Blasius E., Klein W., Schon U., *J. Radioanal. Nucl. Chem.*, **89** (1985), 389.
10. Randolph R.B., *Appl. Radiat. Isot.*, **26** (1971), 9.
11. Vajda N., Ghods-Esphahani A., Cooper E., Danesi P.R., *J. Radioanal. Nucl. Chem. Art.*, **162** (1992), 307.
12. Gerstmann U., Schimmack W., *Radiat. Environ. Biophys.*, **45** (2006), 187.
13. Alan J.R., John V.B., Amita P., Karl B., *J. Contam. Hydrol.*, **79** (2005), 1.
14. Lonin A.Y., A Krasnopyorova P., *Nucl. Phys. Inv.*, **5** (2004), 82.
15. Anna J., Byeong-Heon J., Hoek M.V., *J. Nanopart. Res.*, **11** (2009), 1795.
16. Rakoczy R.A., Traa Y., *Micropor. Mesopor. Mater.*, **60** (2003), 69.
17. Khatamian M., Alaji Z., Khandar A.A., *J. Iran. Chem. Soc.*, **8** (2011), 44.
18. Hirofumi F. Qi, K., Kenta O., *J. Mater. Chem.*, **9** (1999), 319.
19. Shen Y.F., Zerger R.P., DeGuzman R.N., Suib S.L., McCurdy L., Potter D.I., OYoung C.L., *Science*, **23** (1993), 511.
20. Alfaro S., Rodriguez C., Valenzuela M.A., Bosch P., *Mater. Lett.*, **61** (2007), 4655.
21. Cao H., Suib S.L., *J. Am. Chem. Soc.*, **116** (1994), 5334.
22. Jahangirian H., *Dig. J. Nanomater. Bios.*, **8** (2013), 1405.
23. Yamamoto T., Apiluck E., Kim S., Ohmori T., *J. Ind. Eng. Chem.*, **13** (2007), 1142.
24. Yang S., Li Q., Wang M., *Micropor. Mesopor. Mater.*, **87** (2006), 261.
25. Kim S.O., Park E.D., Ko E.Y., *US Pat. No.* 016 25 57 (2006).
26. Banerjea R., *Ind. Med. Gaz.*, **85** (1950), 214.
27. Richter M., Berndt H., Eckelt R., Schneider M., Fricke R., *Catal.*, **54** (1999), 531.
28. Richter M., *J. Catal.*, **206** (2002), 98.
29. Sadeghi M., Hosseini M.H., *J. Nano. Struc.*, **2** (2013), 439.
30. Sadeghi M., Shahdadi M.R., Toolabi H., Husseini M.H., *J. Appl. Chem.*, **3** (2012), 77.
31. Patterson A., *Phys. Rev.*, **56** (1939), 978.
32. Currie L.A., *Anal. Chem.*, **40** (1968), 586.

AUTHOR (S) BIOSKETCHES

Meysam Sadeghi, *M.Sc., Young Researchers and Elite Club, Ahvaz Branch, Islamic Azad University, Ahvaz, Iran*
Email: meysamsadeghi45@yahoo.com

Sina Yekta, *M.Sc., Department of Chemistry, Faculty of Basic Sciences, Islamic Azad University, Qaemshahr Branch,*
Qaemshahr, Iran

Hamed Ghaedi, *Ph.D., Department of Chemistry, Faculty of Basic Sciences, Bu-Ali Sina University, Hamedan, Iran*

Esmaeil Babanezhad, *Ph.D., Department of Chemistry, Faculty of Basic Sciences, Sharif University of Technology, Tehran, Iran*